



Spectral tuning of light-harvesting complex II in the siphonous alga *Bryopsis corticulans* and its effect on energy transfer dynamics



Parveen Akhtar^{a,c}, Paweł J. Nowakowski^b, Wenda Wang^d, Thanh Nhut Do^b, Songhao Zhao^d, Giuliano Siligardi^e, Győző Garab^{a,f}, Jian-Ren Shen^{d,g}, Howe-Siang Tan^{b,*}, Petar H. Lambrev^{a,*}

^a Biological Research Centre, Szeged, Hungary

^b Division of Chemistry and Biological Chemistry, School of Physical and Mathematical Sciences, Nanyang Technological University, Singapore

^c ELI-ALPS, ELI Nonprofit Ltd., Szeged, Hungary

^d Photosynthesis Research Centre, Chinese Academy of Sciences, Beijing, China

^e Diamond Light Source Ltd., Harwell Science and Innovation Campus, Didcot, Oxfordshire OX11 0DE, UK

^f Department of Physics, Faculty of Science, University of Ostrava, Czech Republic

^g Research Institute for Interdisciplinary Science, Graduate School of Natural Science and Technology, Okayama University, Okayama, Japan

ARTICLE INFO

Keywords:

Circular dichroism
Light-harvesting complexes
Marine algae
Photosynthesis
Time-resolved spectroscopy
Two-dimensional spectroscopy

ABSTRACT

Light-harvesting complex II (LHCII) from the marine green macroalga *Bryopsis corticulans* is spectroscopically characterized to understand the structural and functional changes resulting from adaptation to intertidal environment. LHCII is homologous to its counterpart in land plants but has a different carotenoid and chlorophyll (Chl) composition. This is reflected in the steady-state absorption, fluorescence, linear dichroism, circular dichroism and anisotropic circular dichroism spectra. Time-resolved fluorescence and two-dimensional electronic spectroscopy were used to investigate the consequences of this adaptive change in the pigment composition on the excited-state dynamics. The complex contains additional Chl *b* spectral forms – absorbing at around 650 nm and 658 nm – and lacks the red-most Chl *a* forms compared with higher-plant LHCII. Similar to plant LHCII, energy transfer between Chls occurs on timescales from under hundred fs (mainly from Chl *b* to Chl *a*) to several picoseconds (mainly between Chl *a* pools). However, the presence of long-lived, weakly coupled Chl *b* and Chl *a* states leads to slower exciton equilibration in LHCII from *B. corticulans*. The finding demonstrates a trade-off between the enhanced absorption of blue-green light and the excitation migration time. However, the adaptive change does not result in a significant drop in the overall photochemical efficiency of Photosystem II. These results show that LHCII is a robust adaptable system whose spectral properties can be tuned to the environment for optimal light harvesting.

1. Introduction

Bryopsis corticulans (*B. corticulans*) is a marine green macroalga, growing in the rocky intertidal shores in the form of a single-cell thallus with tubular filament siphons. Its photosynthetic apparatus, similar to other species in the order *Bryopsidales*, is adapted for optimal utilization of the predominant blue-green light available under water and may be modulated in response to fast changing light environments [1]. The spectral adaptation involves changes in the pigment composition of light-harvesting complex II (LHCII) – the membrane-intrinsic chlorophyll (Chl) *a/b*-binding peripheral antenna of Photosystem II (PSII). The peculiar structural and functional characteristics of the *B. corticulans* antenna system make it a useful model to understand the design principles of photosynthetic light harvesting and photoprotection [2,3].

At present, there is no crystallographic structure of LHCII from *B. corticulans* and information about the molecular structure and pigment composition is obtained from biochemical and spectroscopy analyses. Although *B. corticulans* is more distant to plants than other green algae such as well-studied *Chlamydomonas reinhardtii*, its Lhcbm apoprotein has >70% sequence identity with the major LHCII (Lhcb1–3) in higher plants and is expected to possess a similar structure with three transmembrane α -helical regions [4–6]. Thus, the key sequences and residues responsible for maintaining the structure and trimerization of LHCII are largely conserved in the siphonous green algae, as are all the carotenoid and Chl binding ligands. In spite of the high degree of homology, however, marked differences are found in the pigment composition. Instead of the xanthophylls lutein and violaxanthin present in higher plants, *B. corticulans* contains siphonaxanthin and

* Corresponding authors.

E-mail addresses: HoweSiang@ntu.edu.sg (H.-S. Tan), lambrev.petar@brc.hu (P.H. Lambrev).

<https://doi.org/10.1016/j.bbabio.2020.148191>

Received 23 October 2019; Received in revised form 11 March 2020; Accepted 13 March 2020

Available online 20 March 2020

0005-2728/© 2020 The Authors. Published by Elsevier B.V. This is an open access article under the CC BY license (<http://creativecommons.org/licenses/by/4.0/>).

siphonoin – unique keto-carotenoids [5–7] which are more reminiscent of the carotenoids found in the light-harvesting antenna complexes of red algae and diatoms. Siphonoin and siphonaxanthin significantly enhance the absorption of green and blue-green light. The centrally located xanthophylls – normally luteins in LHCII of higher plants [8] – are essential for the folding and structural stabilization of the complex. The amino acid sequence of the Lhcbm proteins in *B. corticulans* is altered to accommodate the large hydroxyl group of siphonaxanthin and the large ester group of siphonoin [4–6].

The total number of Chls in LHCII of *B. corticulans* is the same as in plant LHCII – 14. However, instead of eight Chl *a* and six Chl *b*, LHCII of *B. corticulans* binds six Chl *a* and eight Chl *b* [5]. In spite of the exchange of two Chls *a* to *b*, the amino acid ligands to the chlorin rings are the same in the two types of LHCII, suggesting that the ligand environment for Chl *a* and *b* is somewhat flexible. This is in agreement with in vitro reconstitution experiments showing that Chl *a* and *b* can occupy the same binding sites [9,10]. The higher Chl *b/a* ratio also contributes to the absorption of shorter-wavelength light in the region 600–660 nm [1].

Nakayama and coworkers [11,12] investigated the Chl spectral forms and the excitation energy transfer (EET) dynamics in LHCII of a related organism, *B. maxima*. Steady-state and time-resolved fluorescence analysis revealed efficient EET from the carotenoids siphonoin and siphonaxanthin to Chl *a*, whereas EET to Chl *b* was not observed. In contrast to LHCII from spinach, Chl *b* emission was detected in *B. maxima* LHCII upon direct excitation in the Chl *b* region at low temperature (77 K). The authors concluded that a fraction of Chl *b*, albeit small, is unable to transfer energy to Chl *a* at this temperature. This poses the question whether spectral adaptation in the algal LHCII comes at a price of compromising the efficiency of EET. One of the most potent techniques for resolving the dynamics of EET is two-dimensional electronic spectroscopy (2DES), mapping the transient absorbance changes in femtoseconds to nanoseconds time range with simultaneous resolution of the excitation (“pump”) and detection (“probe”) wavelength [13–15]. Circular dichroism (CD) and anisotropic CD (ACD) spectroscopy have recently been proven useful for identifying the exciton states responsible for the spectral features and EET in plant LHCII [16].

Here we present a comprehensive spectroscopic characterization of LHCII isolated from *B. corticulans*, a green macroalga closely related with *B. maxima*, aimed at better understanding the consequences of the pigment composition changes, in comparison with higher-plant LHCII, on the photophysical properties of the antenna. Steady-state absorption, fluorescence, linear dichroism (LD), CD and ACD spectra showed that at least two Chl *a* sites in higher-plant LHCII are occupied by Chl *b* in *B. corticulans*, decreasing the absorption at long wavelengths (674 and 679 nm) and increasing short-wavelength absorption (650 and 658 nm). Time-resolved fluorescence and 2DES showed that overall EET remains highly efficient despite the presence of relatively long-lived Chl *b* forms and slightly slower exciton equilibration dynamics in the Chl *a* domain of *B. corticulans* LHCII.

2. Materials and methods

2.1. Sample preparation

B. corticulans was collected from intertidal coastal areas around Qingdao, China and LHCII was isolated and purified as described in [5]. Detergent-solubilized LHCII was embedded into native thylakoid lipid membranes according to the protocol of Akhtar et al. [17].

2.2. Absorption, LD, CD and ACD spectroscopy

Absorption and CD spectra in the range of 350–750 nm were recorded at room temperature (RT) with a Thermo Evolution 500 spectrophotometer and a Jasco J-815 spectropolarimeter, respectively. LHCII samples in solution were diluted in 20 mM Tricine buffer

(pH 7.8) with 0.03% n-dodecyl β -D-maltoside (β -DDM) to an absorbance of one at the red maximum. Measurements were performed in a standard glass cell of 1-cm optical path length. Synchrotron-radiation (SR) CD spectra in the near and far UV region were measured at the B23 CD beamline of the Diamond synchrotron (UK). For SR CD measurements, the samples were placed in 0.2 mm fused silica cells.

LD and ACD spectra were recorded from reconstituted LHCII membranes macroscopically aligned by polyacrylamide gel compression and by drying on a quartz surface under N_2 gas stream as described in Akhtar et al. [16]. ACD spectra were recorded in face-aligned orientation, with the measuring beam parallel to the membrane normal, and LD spectra were recorded in edge-aligned orientation (with the membrane plane parallel/perpendicular to the beam polarization).

2.3. Steady-state fluorescence spectroscopy

Fluorescence emission spectra at 77 K were recorded with a Fluorolog 3 double-monochromator spectrofluorometer (Horiba Jobin-Yvon, USA). 40 μ l of LHCII solution with absorbance of 0.3 at the red maximum were evenly placed onto a Whatman GF/C glass microfiber filter and immersed in liquid nitrogen in a Dewar glass vessel. Spectra were recorded in the range of 600–800 nm with 436 nm and 475 nm excitation light and 5 nm excitation/emission spectral bandwidth and corrected for the spectral response of the detector. RT fluorescence spectra were recorded with a Jasco FP-8500 spectrofluorometer. The samples were diluted to absorbance of 0.01 at the red maximum and placed in a 1-cm quartz cell.

2.4. Time-resolved fluorescence

Fluorescence decays were measured at RT by time-correlated single-photon counting using a FluoTime 200/PicoHarp 300 instrument (Picoquant, Germany). The source of excitation was a Fianium WhiteLase Micro (NKT Photonics, UK) supercontinuum laser, providing white-light pulses at a repetition rate of 20 MHz. The samples were diluted to an absorbance of 0.03 at the excitation wavelength in a 1.5-mm pathlength flow cell and continuously circulated during the measurement to avoid repeated excitation of the same sample volume. The excitation wavelength was set to either 460 nm or 633 nm by passing the laser beam through an excitation monochromator and a band-pass filter and the pulse energy was adjusted to \sim 0.1 pJ. Fluorescence decays were recorded at wavelengths between 656 and 744 nm with 8 nm steps and binned in 4-ps time channels. The instrument response function (IRF) was measured using 1% Ludox (colloidal silica) as scattering medium. The IRF width was \sim 50 ps at the excitation wavelength. The fluorescence decays were subjected to global multi-exponential lifetime analysis routine with IRF deconvolution to obtain lifetimes and decay-associated emission spectra (DAES) using MATLAB routines created in-house.

2.5. Two-dimensional electronic spectroscopy

Fourier-transform femtosecond 2DES was performed at 295 K (RT) and 77 K in a partially collinear “pump-probe” geometry using an experimental setup described in [18]. Briefly, a two-pulse train of interaction pulses (pump/excitation pulses) of 35 fs duration with controllable inter-pulse delay time and phase difference are obtained by passing the output of a non-collinear parametric amplifier (TOPAS, Light Conversion) through an acousto-optic programmable dispersive filter (AOPDF) pulse shaper (Dazzler, Fastlite). The spectra of the excitation pulses are centred at 670 nm, coinciding with the Chl *a* Q_y absorption band of LHCII (Supplementary Fig. S1). A white-light supercontinuum pulse generated in a 2-mm sapphire window is used as the third interaction pulse (probe/detection) after compressing with a pair of chirped mirrors. The transient absorption of the probe is then measured along the λ_r axis. The cross-correlation width of the

excitation and probe pulses was 70 fs (FWHM) or less. The time delay τ between the two excitation pulses was scanned between 0 and 150 fs with 3-fs steps for RT measurements and between 0 and 378 fs with 6-fs steps for 77 K measurements. The 2D photon echo signals were recorded by utilizing a 1×2 phase cycling scheme in a partially rotating frame of reference [19]. The probe pulse was plane-polarized at the magic angle (54.7°) with respect to the polarization of the excitation pulses. The signals (2D interferograms) were Fourier-transformed along τ to obtain 2D electronic spectra in the frequency/wavelength domain (with excitation/detection wavelengths λ_e/λ_d). The waiting time (T_w) between the excitation and probe pulses was scanned from -100 fs to 100 ps in a quasilogarithmic progression. The excitation pulse energy was attenuated to 1–1.5 nJ, equivalent to $\sim 2 \times 10^{13}$ photons/cm²/pulse, to obtain maximal transient absorption signal of 1.5 and 2 mOD for RT and 77 K, respectively. The average number of excitations per LHCII trimer was approximately estimated to be 0.04–0.06.

For 2DES measurements at RT, the LHCII samples were diluted in degassed buffered medium (pH 7.8) containing 20 mM tricine and 0.03% β -DDM to absorbance of 0.3 at 675 nm (1 mm path length). The sample was continuously circulated during the measurement. For 77 K measurements the LHCII samples were diluted in degassed buffered medium (pH 7.8) containing 60% (v/v) glycerol, 20 mM tricine and 0.03% β -DDM. The suspension was placed in a cell between two sapphire windows separated by a 0.5-mm Teflon spacer shielded with cryogenic grease to absorbance of 0.3 at 675 nm. Temperature was controlled by a liquid-nitrogen-cooled vacuum cryostat (Janis) with BaF₂ windows.

3. Results

3.1. Absorption and fluorescence spectra

The absorption spectra of LHCII trimers isolated from *B. corticulans* solubilized with β -DDM are compared with LHCII isolated from pea (*Pisum sativum*) in Fig. 1. The RT absorption spectra have two characteristic peaks in the Soret region, at 437 nm and 475 nm, and two in the Chl Q_y region, 672 nm and 651 nm, primarily attributed to Chl *a* and Chl *b*, respectively. The peak positions and their amplitudes slightly differ between *B. corticulans* and *P. sativum* owing to the different pigment composition of the two species. The positive peaks at 655 nm and 478 nm in the difference absorption spectrum testify to a higher Chl *b* content of *B. corticulans*, and, conversely, the negative peaks at 680 nm and 430 nm indicate lower Chl *a* content. The broad absorption band at 532 nm in *B. corticulans* is due to the carotenoids siphonin and siphonaxanthin [5]. The absorption spectrum of *B. corticulans* LHCII at 77 K (Fig. 1b) contains two resolved peaks in the Chl *b* Q_y region – at 650 and 658 nm. The difference spectrum with *P. sativum* shows negative peaks at 679 nm and 674 nm and positive peaks at 650 nm and

658 nm.

Fluorescence emission spectra of LHCII from *B. corticulans* and *P. sativum* at RT and 77 K are shown in Fig. 2. Reflecting the blue-shifted maximum in the absorption spectrum, the emission of *B. corticulans* is shifted by 2 nm to shorter wavelengths. The spectra also show higher emission from Chl *b* at RT – 16% relative fluorescence intensity at 655 nm, compared to 9% in the spectrum from *P. sativum*. There is virtually no Chl *b* emission at 77 K.

3.2. CD, ACD and LD spectra

The CD and ACD spectra of LHCII from *B. corticulans* measured in the visible wavelength region are shown in Fig. 3. Note that for the measurement of ACD and LD spectra, the complex was embedded in reconstituted membranes. The CD spectrum of reconstituted LHCII membranes (Supplementary Fig. S2) is not significantly different from that of LHCII solubilized in β -DDM (Fig. 3a). In the red region, the CD spectrum is characterized by two negative (651 and 681 nm) and one positive band (665 nm) associated with the Q_y exciton states of Chl *b* and *a*. The CD in the Soret region is dominated by two negative bands (475 nm and 492 nm) and two positive bands (445 nm and 484 nm). *B. corticulans* and higher-plant (*P. sativum*) LHCII share similar spectral features, both in the ultraviolet and in the visible wavelength region (Supplementary Fig. S2). *B. corticulans* shows stronger CD in the Q_y band of Chl *b*, 651 nm, stronger positive CD bands at 445 nm and 484 nm and an additional negative CD band at 532 nm. The CD bands associated with Q_y transitions of Chl *a* are blue-shifted compared to higher-plant LHCII, in agreement with the blue-shifted absorption maximum.

The face-aligned ACD spectrum enhances excitonic CD bands wherein the electronic transition dipole moment is predominantly parallel to the membrane plane (Fig. 3b). The ACD spectrum has intense positive peaks at 445 nm and 484 nm – which is characteristic of higher-plant LHCII as well [16]. Further, bands at 586, 607 and 637 nm are clearly visible in the ACD spectrum but barely or not at all detectable in the isotropic CD. On the other hand, the negative bands at 431 and 473 nm, observed in the CD spectra, are suppressed in the ACD spectrum, signifying that the associated transition dipole moments are close to perpendicular to the membrane plane. A notable difference between the ACD spectra of the algal and the higher-plant LHCII is that the positive band at 680 nm in the latter is not observed in *B. corticulans* – the red-most ACD band is negative in the algal spectrum (see Discussion). On the other hand, *B. corticulans* shows an additional positive ACD band at 454 nm. ACD spectra were also recorded from uniaxially compressed gels in the face-aligned position as a control (Supplementary Fig. S3). The spectra were virtually identical to the spectra of dehydrated lipid films.

The major bands in the face-aligned ACD spectrum – at 445 and

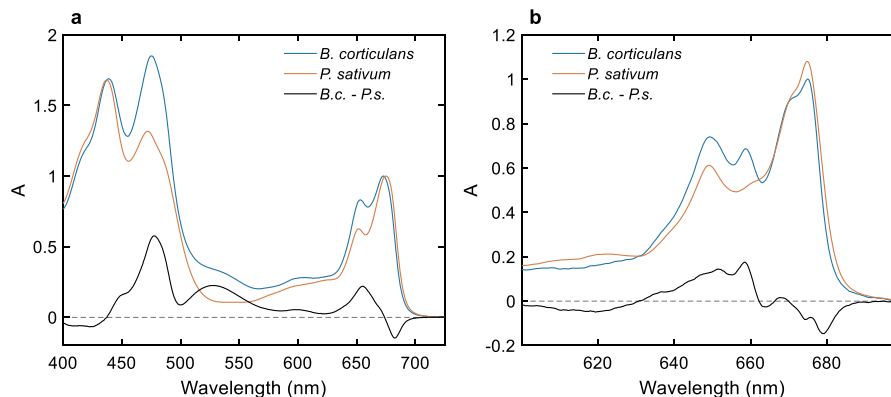


Fig. 1. Absorption spectra of LHCII isolated from *B. corticulans* and *P. sativum* solubilized in 0.03% β -DDM at RT (a) and 77 K (b). The black curve shows the difference spectrum *B. corticulans* minus *P. sativum*.

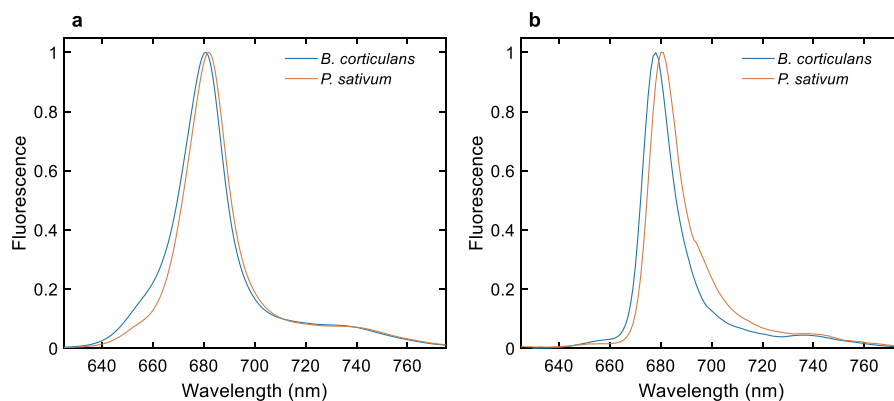


Fig. 2. Fluorescence emission spectra of LHCII from *B. corticulans* and *P. sativum* at RT (a) and 77 K (b), with excitation at 475 nm. The spectra are normalized to the maximum emission.

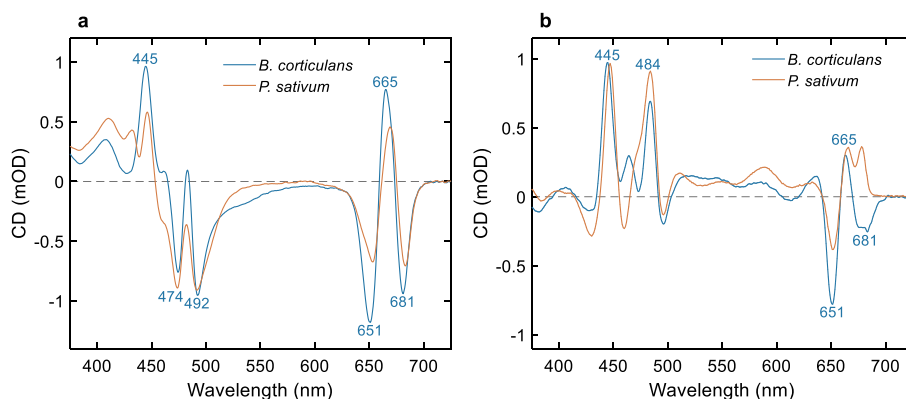


Fig. 3. CD and ACD spectra of LHCII from *B. corticulans* and *P. sativum* (a) CD spectra of LHCII solubilized in 0.03% β -DDM and (b) ACD spectra of membranes oriented in dehydrated films. The spectra are plotted in units of $\Delta A \times 10^{-3}$ (mOD) and normalized to unity isotropic absorbance at 675 nm.

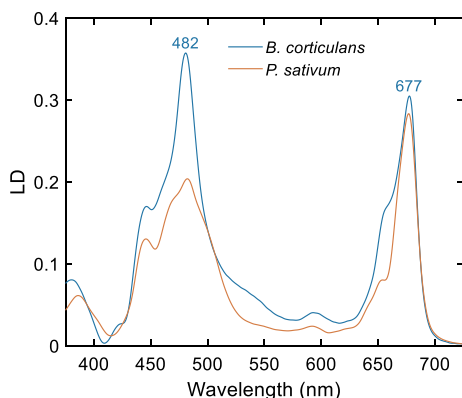


Fig. 4. LD spectra of LHCII from *B. corticulans* and *P. sativum* measured from membranes in a squeezed polyacrylamide gel in edge-aligned orientation. The spectra are normalized to unity isotropic absorbance at 675 nm.

484 nm – are correlated with positive peaks in the LD spectrum of edge-aligned LHCII membranes (Fig. 4), confirming that the contributing transition dipole moment is preferentially parallel to the membrane plane. Comparison with the LD spectrum of plant LHCII, highlights the additional chlorophyll *b* forms in *B. corticulans*.

3.3. Time-resolved fluorescence

The fluorescence decay kinetics of LHCII of *B. corticulans* was recorded by time-correlated single photon counting at several emission wavelengths (Fig. 5). Global multiexponential analysis of the decays at

emission wavelengths 664–744 nm required three decay lifetimes to fit the data (Supplementary Fig. S4) – a major lifetime of 4.5 ns, having 90% contribution, and two shorter lifetimes (120 ps and 1.2 ns). Interestingly, this results in an average fluorescence lifetime of 4.0 ns – longer than higher-plant LHCII, which was found to be 3.5–3.6 ns, consistent with previous reports [20,21]. The decay-associated emission spectra (DAES) are nearly identical for all three components (Fig. 5). It can be concluded that upon excitation at 633 nm (exciting both Chl *a* and *b*), EET is faster than the time resolution of the instrument (approx. 20 ps). The same conclusion can be drawn from an inspection of the time-resolved spectra and the decay traces at different wavelengths (Supplementary Fig. S5). LHCII embedded in liposomes exhibits multiexponential kinetics with shorter decay lifetimes and the spectra show enhanced emission above 700 nm (Supplementary Fig. S6), similar to LHCII from higher plants [22]. In this case, global analysis resolves an 80-ps lifetime component with a positive peak in the DAES at 680 nm and negative peak at \sim 700 nm. Therefore, the component likely represents the appearance (via EET) of states emitting in the far-red region that can be assigned to mixed exciton-charge-transfer states.

3.4. Two-dimensional electronic spectroscopy

3.4.1. Room temperature 2D electronic spectra

The 2D electronic spectrum is a correlation map of two frequencies or wavelengths for a given waiting time T_w . Generally, the negative absorptive signal at excitation wavelength λ_e and detection wavelength λ_d (denoted $\lambda_e \rightarrow \lambda_d$) is proportional to the population, at time T_w , of states absorbing at λ_e , given that the initial excitation was at λ_e . Fig. 6 shows RT 2D electronic spectra of detergent solubilized LHCII from *B.*

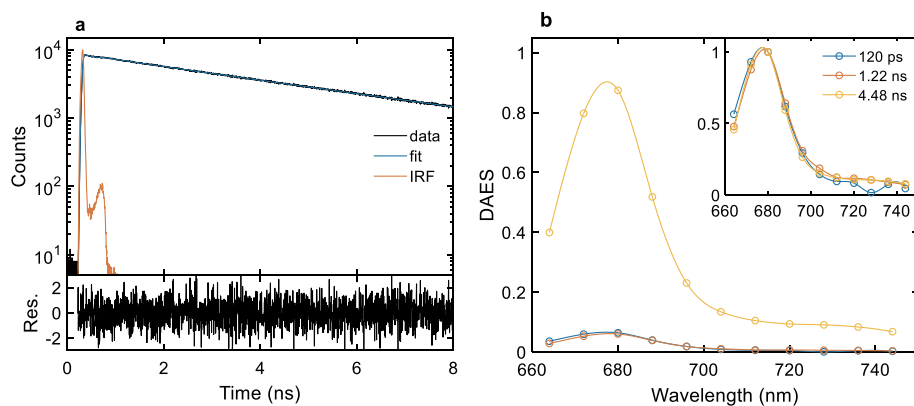


Fig. 5. Time-resolved fluorescence spectroscopy of detergent solubilized LHCII of *B. corticulans*. (a) Fluorescence decay trace at 680 nm emission (black), three-exponential fit (blue), IRF (red) and weighted residuals (lower subplot). (b) Decay-associated emission spectra obtained from three-exponential global analysis of the decays at 664–744 nm. The inset shows normalized decay-associated spectra.

corticulans recorded at several distinct T_w . The total spectral width along the vertical axis (λ_r) is determined by the overlap of the excitation pulse spectrum and the LHCII absorption spectrum (Supplementary Fig. S1). At early waiting times ($T_w = 100$ fs), the negative signal (from ground-state bleaching and stimulated emission) is predominantly aligned along the diagonal, representing population of states directly excited by the pump pulse (Fig. 6a). Off-diagonal signals are also observed in the region $\lambda_r = 650$ –670 nm and $\lambda_r = 660$ –680 nm, indicating very fast exciton relaxation among strongly coupled Chl domains. In the evolution of the 2D spectrum from 100 fs to 1 ps (Fig. 6a and b, respectively), the diagonal signal around 650 nm decays (by about 70%) while off-diagonal signals gain intensity.

The rapid decay of the 650-nm diagonal signal is shown by the time course in Fig. 7. The 665-nm diagonal trace decays markedly slower while the off-diagonal signal from 650 nm to 665 nm reaches its maximum value in <300 fs and decays thereafter. The time traces and the 2D spectra clearly show significant remaining population of states at around 665–670 nm up to 5 ps. On the other hand, almost no population of states absorbing below 660 nm is detected at this time

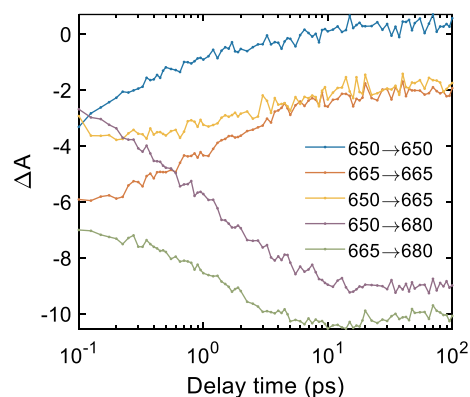


Fig. 7. Waiting-time dependence of the absorptive signal from 0.1 to 100 ps at selected excitation/detection wavelength intersections in the 2D electronic spectra, indicated as $\lambda_r \rightarrow \lambda_r$. Note the logarithmic time scale.

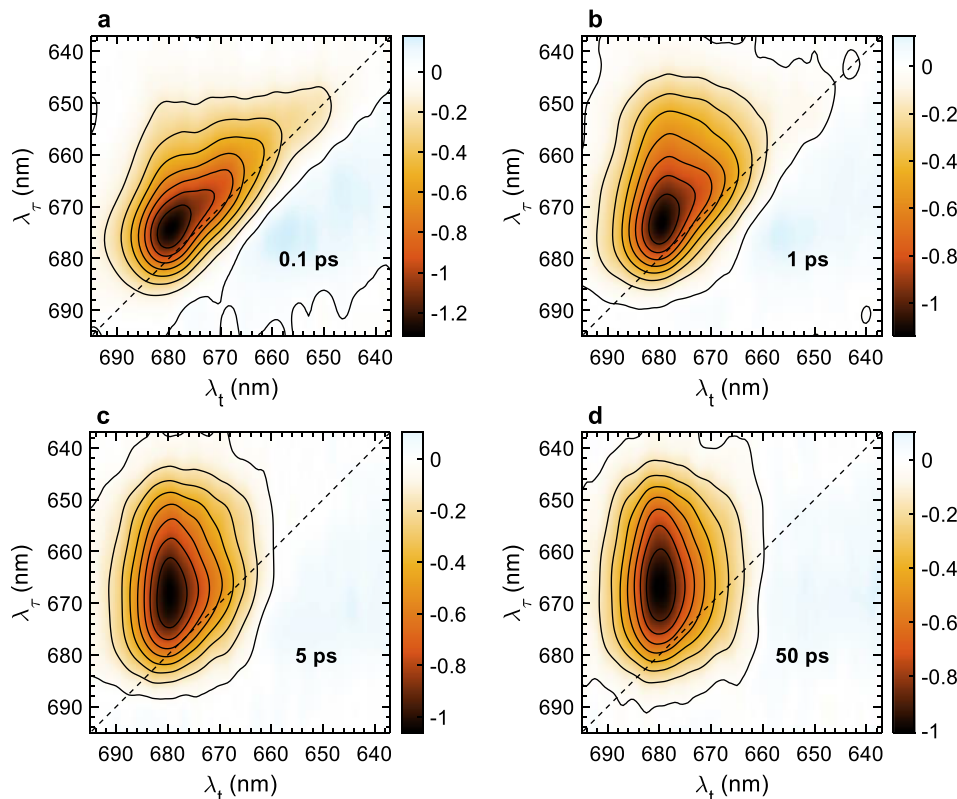


Fig. 6. Representative purely absorptive 2D spectra of detergent solubilized LHCII (*B. corticulans*) recorded at RT with excitation pulses centred at 670 nm and selected waiting times (0.1, 1, 5 and 50 ps). The symbols λ_r and λ_t indicate excitation and detection wavelengths, respectively. Yellow-red colours code the negative ground-state bleach/stimulated emission signal with contour lines at every 12.5% intensity.

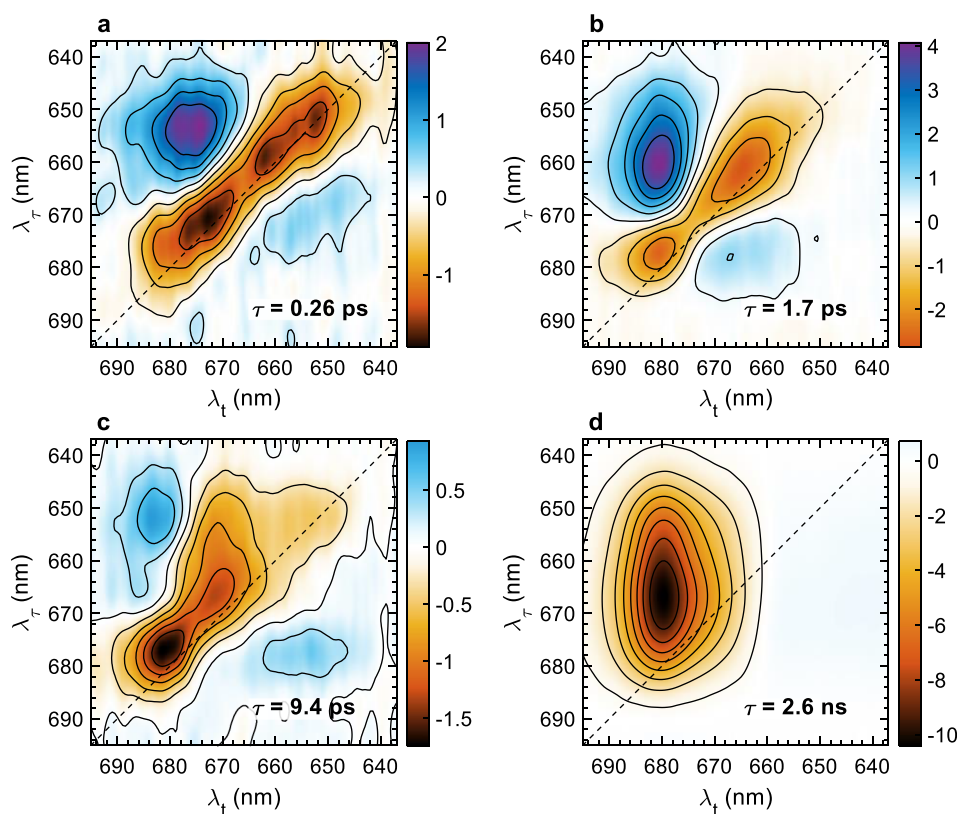


Fig. 8. 2D decay-associated spectra of LHCII obtained from four-component global lifetime analysis of 2DES data collected at RT. Red/blue colours represent negative/positive amplitudes (decay/rise of the negative absorptive signal). Note the different colour coding of the signal amplitude. (For interpretation of the references to colour in this figure legend, the reader is referred to the web version of this article.)

(Fig. 6c). With the decay of the 665-nm diagonal trace and the 650–665-nm off-diagonal trace, a corresponding rise of the 665–680-nm trace is observed showing that excitations are transferred to lower-energy states. Thus, the spectral evolution generally shows a multistep cascade with rapid EET (mostly within 1 ps) from Chl *b* to the intermediate wavelength region at 660–670, followed by slower dynamics to the low-energy Chl *a* states. Virtually all EET ceases by 20 ps. The 2D spectra beyond this waiting time are centred at $\lambda_t = 680$ nm and exhibit no correlation between excitation and detection wavelengths (Fig. 6d), which signifies that a thermal equilibrium among all states has been reached.

To obtain a quantitative measure of the EET timescales and associated pathways, the time-resolved 2DES data were subjected to global multiexponential lifetime analysis [23]. Four lifetime components were necessary for a satisfactory fit. The 2D decay-associated spectra (2D DAS), shown in Fig. 8, describe the spectral changes occurring in the 2D electronic spectra with the corresponding lifetimes. Negative or positive amplitudes primarily indicate that the ground state bleach/stimulated emission signal decays or rises, respectively, on a given timescale. The shortest resolved lifetime (260 fs) is characterized by the decay of the diagonal signals (negative amplitudes) along the entire probed region with local maxima at 652 and 660 nm, and the corresponding rise (positive amplitudes) of off-diagonal signals at $\lambda_t = 672$ –675 nm (Fig. 8a). The second 2D DAS (1.7 ps) (Fig. 8b) shows the decay of states at around 662–665 nm, which are either directly excited (on the diagonal) or populated via EET from upper-lying states ($\lambda_t = 650$ –660 nm) and the corresponding rise of low-energy Chl *a* excitons ($\lambda_t \approx 680$ nm). The slowest EET timescale, 9.4 ps (Fig. 8c), shows decay of diagonal and cross-peak signals at $\lambda_t \approx 670$ nm and further rise of the lowest-energy excitons. A diagonal peak at 650–655 nm is also resolved in the 2D DAS, revealing a small fraction of long-lived Chl *b* states. Overall, 20% of excitations from 650 nm are transferred to the lowest-energy states (680 nm) within 100 fs, 24% on a 260 fs timescale, and the remaining 56% are transferred on a timescale longer than 1 ps – the amplitude-weighted average rise time of the

650 → 680 nm cross-peak is ~ 2 ps.

All three EET components also show uphill pathways as cross-peaks below the diagonal ($\lambda_t < \lambda_\tau$), positioned generally symmetric to the downhill cross-peak but with lower amplitude, as expected from the detailed balance [24]. The final 2D DAS ($\tau \approx 3$ ns) (Fig. 8d) reflects the decay to the ground state. As described above, the shape of the spectrum shows almost no correlation between the excitation and detection wavelengths, indicating that EET is complete and a final, thermally equilibrated state population is reached independent of the initial excitation.

3.4.2. 2D electronic spectra at 77 K

Cooling down to 77 K brings about more spectral details – the lineshapes are significantly narrower and individual peaks become resolved in the 2D electronic spectra (Fig. 9) – around 650, 658, 669 and 677 nm. At early waiting times ($T_w = 100$ fs), all four peaks are along the diagonal line (Fig. 9a). A cross-peak is also observed around $\lambda_\tau = 670$ nm and $\lambda_t = 675$ –678 nm, which is separated from the diagonal peak at 669 nm and probably originates from excitonic coupling between Chl *a* molecules. In the time between 100 fs and 1 ps (Fig. 9a and b, respectively), the 650 and 658-nm peaks practically vanish and corresponding cross-peaks at $\lambda_t \approx 675$ nm are visible. This indicates that EET from the high-energy Chl *b* band to Chl *a* occurs at a rate comparable to that observed at RT.

The 669-nm peak retains 70% of its intensity at 1 ps, the remaining 30% apparently being transferred to 674 nm. The 669-nm peak is detectable even after 5 ps (Fig. 9c), at about 23% of its initial amplitude. By 50 ps (Fig. 9d), all peaks are centred around $\lambda_t = 677$ nm, which is the terminal excited state. In contrast to the RT measurements, there is still a pronounced correlation between excitation and detection wavelengths at long waiting times. This is visualized by the horizontal cuts of the spectra at λ_τ in the range 676–680 nm (Supplementary Fig. S7). In other words, the final exciton state at 77 K, depicted by the diagonal peak at 677 nm, is inhomogeneously broadened.

More details about the EET at 77 K can be seen in the selected kinetic traces in Fig. 10. For instance, the 652-nm diagonal trace (blue

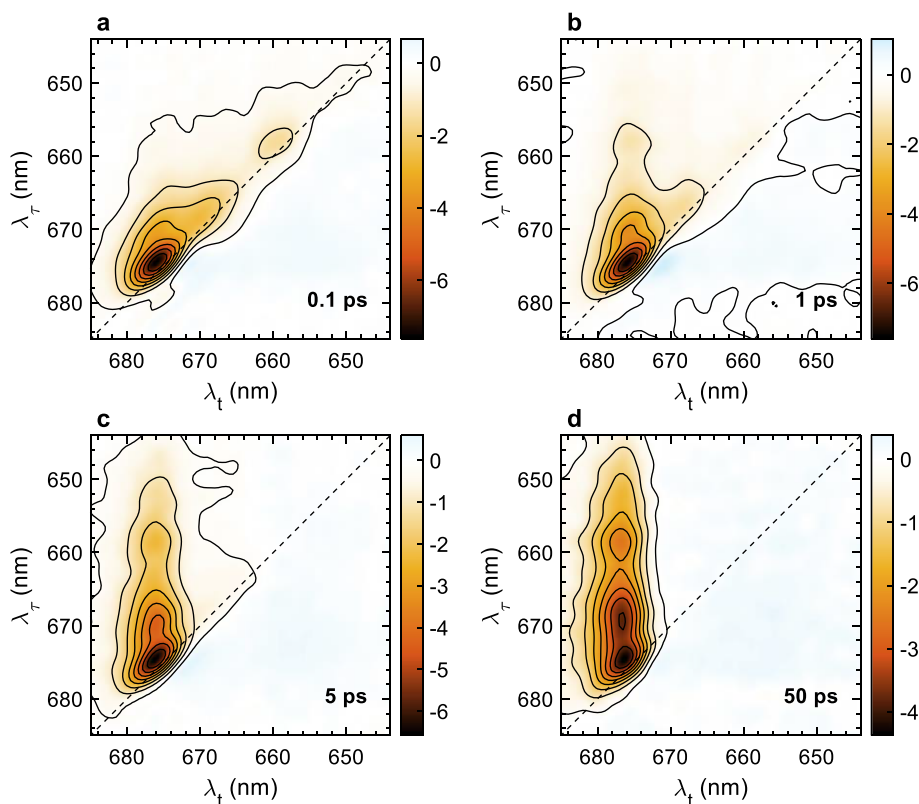


Fig. 9. Representative purely absorptive 2D electronic spectra of detergent solubilized LHCII trimers recorded at 77 K with excitation pulses centred at 670 nm, at selected waiting times T_w as indicated. The symbols λ_r and λ_t indicate excitation and detection wavelengths, respectively.

curve, Fig. 10a) decays slightly faster than the 658-nm trace (Fig. 10b); initial excitation at both wavelengths results in the population of states around 670 nm (red curves), which grows until 1 ps and thereafter decays, giving rise to lower-energy states. The transients also reveal slow relaxation of states around 674 nm occurring on a timescale longer than 10 ps (yellow curves). The population of the lowest-energy states (purple) steadily grows until 30–40 ps, at which point decay processes prevail.

The 2D DAS resulting from four-exponential fitting of the 2D electronic spectra at 77 K are plotted in Fig. 11. The first three 2D DAS (Fig. 11a, b and c) with lifetimes of 0.5, 2.7 and 15 ps are associated with EET as seen by the decaying diagonal states and corresponding rise of cross-peaks, mainly at longer detection wavelengths. The final lifetime in the nanoseconds range represents decay to the ground state. The shortest resolved lifetime of 0.5 ps is associated with decay of the

shorter-wavelength peaks resolved in the 2D electronic spectra – at 650, 658 and 669 nm – giving rise to states at detection wavelengths between 665 and 675 nm. Also visible is the decay of a 652 → 658-nm cross-peak signal, i.e. relaxation of the 658-nm states, which have been populated from states absorbing around 652 nm by very fast EET.

The second 2D DAS (2.7 ps) (Fig. 11b) reflects the subsequent relaxation of excitons at 658 and 669 nm. The negative-amplitude cross-peaks at the corresponding detection wavelengths, 650 → 658 nm, 653 → 669 nm, 658 → 669 nm, show that these intermediate states bridge the EET from the high-energy Chl *b* to Chl *a*. Exciton equilibration in the 670–675 nm region also occurs on this timescale, with well resolved downhill and uphill cross-peaks.

The slowest EET lifetime of 15 ps (Fig. 11c) is associated mainly with EET between the lowest Chl *a* states in the 674–678 nm region. However, diagonal peaks at 664–669 nm and at 650 nm are also visible

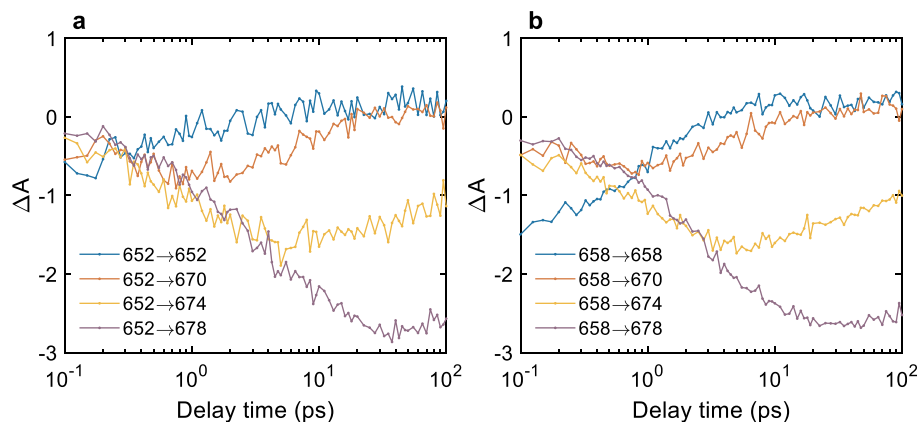


Fig. 10. Waiting-time dependence of the absorptive signal of LHCII at 77 K, at selected wavelength intersections, indicated as $\lambda_t \rightarrow \lambda_r$, plotted for two excitation wavelengths, 652 nm (a) and 658 nm (b).

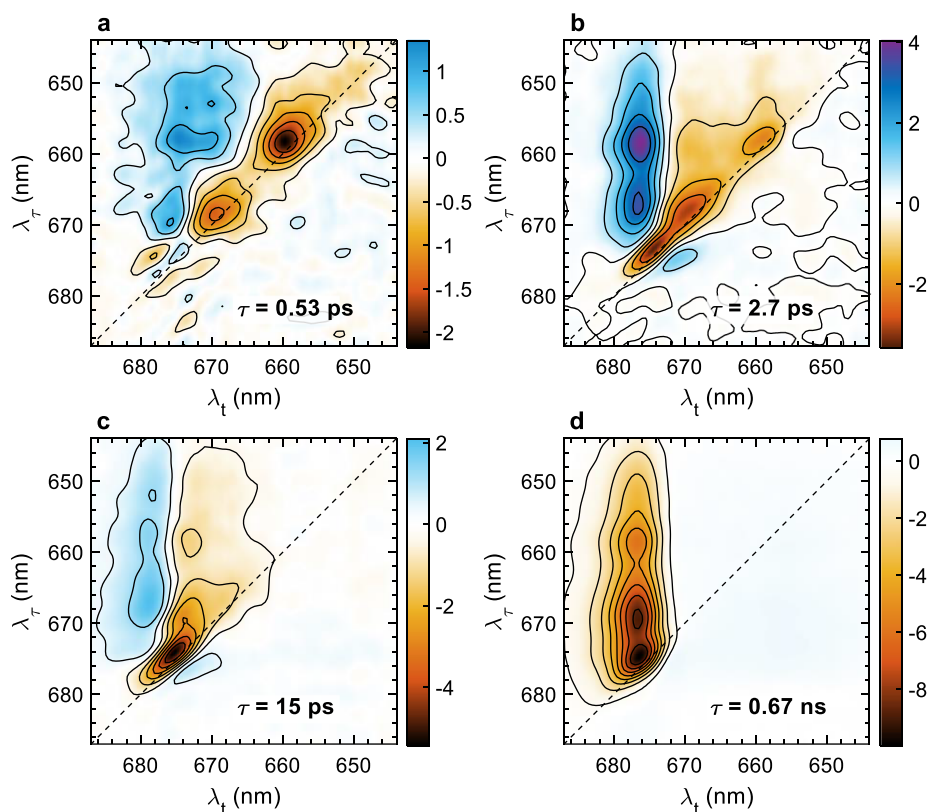


Fig. 11. 2D decay-associated spectra of LHCII at 77 K, obtained from four-component global lifetime analysis of the 2DES data. Red/blue colours represent negative/positive amplitudes (decay/rise of the negative absorptive signal).

(see Fig. S8), showing the existence of weakly coupled Chls, presumably Chl *a* and Chl *b*, respectively. The shape of the final 2D DAS (representing decay to the ground state) is practically identical to the 2D electronic spectrum at $T_w = 50$ ps (see Fig. 9d).

4. Discussion

4.1. Chl spectral forms

The efficiency of light harvesting, and hence of photosynthetic energy conversion, depends on the ability of the light-harvesting antenna to (1) absorb the available radiation, i.e. maximize the cross-section and (2) deliver the energy to the reaction centres without quantum losses, i.e. minimize the EET time. These two criteria are inherently at odds – on one hand, the excitation migration time scales with the antenna size and, on the other, the Förster resonance EET rate decreases as the energy gap between the donor–acceptor chromophores increases. The light-harvesting antenna of *B. corticulans* has an altered carotenoid and Chl composition that enhances the absorption of shorter-wavelength light available below the water surface, when submerged. The carotenoids siphonoin and siphonaxanthin are well suited to absorb green light in the wavelength region between the Soret and Q_y transitions of Chls (Fig. 1) and the efficiency of EET transfer to Chls is higher than 90%, enabling *B. corticulans* to absorb and utilize the green light efficiently under intertidal water [5,25]. *B. corticulans* also binds more Chl *b* at the expense of Chl *a* (compared to higher plants) to harvest blue-green light (460–500 nm), and the consequences of this change on the spectroscopic and EET characteristics of the complex are the primary focus of the present study.

Owing to the high degree of sequence homology and the conservation of all Chl binding sites in Lhcbm from *B. corticulans* and Lhcb from higher plants [5], the folded protein complexes should have a similar secondary and tertiary structure and general pigment

arrangement; this is also corroborated by the virtually identical CD spectra in the UV region (Supplementary Fig. S2). The absorption spectra confirmed that *B. corticulans* binds two extra Chl *b* molecules, giving rise to two positive peaks in the Chl *b* Q_y region of the difference spectra *B. corticulans* minus *P. sativum* (Fig. 1). Because of the different binding sites, the two Chls differ in transition energy – one absorbs at 658 nm and the other around 650 nm. The additional 658-nm spectral form is also clearly resolved in the 2D electronic spectra at RT (Fig. 6) and 77 K (Fig. 9). It must be noted that similar 77 K absorption spectra were reported for *B. maxima*, where the 658-nm Chl form was present and identified by gaussian decomposition analysis but ascribed to Chl *a* [11]. Additional features in the absorption difference spectrum (Fig. 1b) hint that the transition energies of other Chls are perturbed in *B. corticulans*. This is expected as the Chl *a/b* exchange will affect excitonic couplings with neighbouring Chls even if the overall pigment arrangement/conformation is retained. Furthermore, the transition energy of Chls may also be affected by the protein environment surrounding their binding sites [26], since there are slight differences in the residues surrounding the binding sites [5] even though the direct ligands for all are conserved between the green alga and higher plants.

It is interesting to observe that the additional Chls *b* in *B. corticulans* LHCII are at the expense of apparently the lowest-energy form of Chl *a* (679–680 nm). This results in blue-shifted maxima of the linear spectra (absorption, fluorescence, CD). The missing lowest-energy state is also evident in the 2D electronic spectra. Recently, phenomenological modelling of the 2DES data of *P. sativum* LHCII recorded under similar experimental conditions has revealed that the final state at 77 K is a distribution of predominantly two excitons – at 677–678 nm and 679–680 nm [27]. In contrast, the 2D electronic spectra of *B. corticulans* LHCII at long delay times are centred at 677 nm (Fig. 9) – the lowest-energy exciton in this complex. Nakayama and Mimuro [11] fitted a 679-nm component to the absorption spectra of *B. maxima* recorded at 15 °C but the longest-wavelength form at 77 K was at 675 nm (apart

from a substoichiometric broad band at 682 nm). Note that in both *B. corticulans* and plant LHCII, cooling results in a gradual blue shift in the absorption [28] as well as the 2D electronic spectra [24] and an apparent disappearance of the red-most transitions that could be of vibronic nature [29].

Without a high-resolution structural model, we can only speculate about the binding sites of the extra Chl *b* molecules; however, the spectroscopic data presented here reveal that at least one of them is associated with the so-called terminal emitter or the lowest-energy exciton in plant LHCII. Earlier mutagenesis and spectroscopy studies on plant LHCII [26] and the most recent model calculations [30] have assigned the lowest exciton state to Chl *a*612, whereas other models point to *a*610 [31,32]. It is also possible that the latter two Chls change their role as the lowest-energy sink depending on temperature [33,34]. Müh et al. [32] suggested a possible conformational change of the Chl *a*604 site (with respect to the crystal structure) resulting in a red shift. Accordingly, Chls *a*604 and *a*610 may be the lowest-energy sinks in plant LHCII.

ACD spectroscopy can help identify the pigments contributing to spectral features by virtue of generally less crowded spectra [16,35,36] and by linking excitonic bands and the orientation of the underlying transition dipole moments [37]. Corroborating the assignment of Müh et al. [32], the ACD spectra of plant LHCII calculated using their exciton model provided a good qualitative fit of the experimentally measured spectra [16]. Moreover, when Chls *a*604 and *a*610 were omitted from the model, the resultant simulated ACD spectra failed to reproduce a characteristic sign inversion of the ACD at 680 nm. Similarly, if one of the energy sinks is replaced by Chl *b*, the positive ACD band at 680 nm should not be observed. Indeed, the ACD spectra of *B. corticulans* LHCII lack the positive 680 nm band. Provided that the assignment of the lowest-energy sinks in the model of Müh et al. is correct, it would follow that either Chl *a*604 or *a*610 must be replaced by Chl *b* in *B. corticulans*.

4.2. Excitation decay lifetimes

Because excitation energy equilibration in the complex is generally very fast ($\ll 0.1$ ns), the fluorescence of the equilibrated system should decay monoexponentially. The minor contribution of short-lived fluorescence decay components (0.1–1.2 ns) might originate from small subpopulations ($<10\%$ total) of aggregated or dynamically quenched complexes in the sample. Both the average lifetime (4 ns) and the major decay lifetime (4.5 ns) of LHCII from *B. corticulans* are slightly longer than the respective values in higher-plant LHCII but within the range of values observed previously, especially for monomeric LHCII (unpublished data), and can be attributed to the slightly different local environment of the emitting Chls. On the other hand, the pronounced lifetime heterogeneity and reduction of the average fluorescence lifetime in proteoliposomes (Supplementary Fig. S6) is a result of the altered environment – mainly the formation of protein-dense LHCII clusters in the membrane [22,38].

It should be noted that the excitation decay lifetimes reported by 2DES are shorter – 1.4–2.6 ns at RT and 0.6–0.8 ns at 77 K. This apparent inconsistency is mostly due to the short time range of the measurements (0–100 ps). Consequently, short-lived components of even minor amplitudes (Fig. 5) may significantly bias the fit. Additional excitation decay is likely present in the conditions of the 2DES measurements due to singlet annihilation and the presence of glycerol [24]. It remains to be clarified whether the excitation lifetime actually depends on the temperature in the absence of these factors.

4.3. Energy transfer dynamics

The central question of the present investigation is how pigment composition changes in LHCII affect the dynamics and efficiency of energy transfer. In LHCII isolated from plants, EET from Chl *b* to Chl *a* occurs in the range of 0.15–0.5 ps at RT [39–41] and 0.3–0.6 ps at low

temperatures [42–45]. A distinctive characteristic of all LHCII forms is the presence of long-lived Chl forms absorbing in an intermediate region (660–670 nm) between the major Chl *b* and Chl *a* Q_y bands [46,47]. In recent years, several 2DES theoretical modelling studies have revealed further details on the EET dynamics in plant LHCII [for review, see 15]. The lifetime of the intermediate ‘bottleneck’ state as well as the equilibration between the lowest-energy Chl *a* domains and between monomers in the trimers are in the range of several ps. Longer components in the range of 10–20 ps are resolved at low temperatures [24].

In an earlier work, Zhang et al. [48] assumed that excitation equilibration in LHCII from *B. corticulans* occurs with time constants spanning up to 160 ps. The analysis was based mainly on multiexponential fits of the fluorescence decay kinetics recorded at fixed emission wavelengths. While a decay component of comparable lifetime (120 ps) was resolved in the time-resolved fluorescence presented here, the multiwavelength global analysis results are definitive – no EET takes place on such a long timescale and the decay is attributed to a small fraction (5%) of quenched complexes, always present in vitro. Clearly, the time window of EET is considerably shorter than 50 ps (the instrument response width), as is the case with plant LHCII and in concord with the 2DES experiments performed with 35 fs pulses.

The increased Chl *b* emission observed in the fluorescence spectra at RT could mean that some Chl *b* molecules transfer energy to Chl *a* with lower efficiency. However, Chl *b* emission (5–10% intensity relative to Chl *a*) is also observed in RT spectra of higher-plant LHCII – this is a consequence of thermal equilibration and can be expected from the detailed balance condition. The relative increase of Chl *b* emission (at 650–660 nm) in *B. corticulans* is ~ 1.8 -fold higher (Fig. 2), i.e. equivalent to the change in the Chl *b/a* ratio. Moreover, there is no difference between the fluorescence emission spectra upon Chl *a* and Chl *b* excitation (data not shown). All these observations indicate that the Chl *b* emission at RT is due to thermal equilibration. Finally, there are no persistent diagonal peaks in the 2D electronic spectra, which would indicate the presence of energetically uncoupled Chls in the complexes. Therefore, we can conclude with confidence that the light-harvesting complexes are fully functional in the sense that all absorbing chromophores are coupled with high EET efficiency. The very low Chl *b* emission at 77 K (Fig. 2b), which is consistent with the results of Nakayama and Mimuro on *B. maxima* [11], can be attributed to a small, substoichiometric fraction of uncoupled Chl *b* in the samples. Nevertheless, the 2DES data show marked differences in the dynamics of EET in the plant and algal LHCII, as discussed below.

The RT 2D electronic spectra are generally similar to those of higher-plant LHCII obtained with the same experimental setup [15,49]. They show spectral redistribution occurring on different timescales – from several hundred fs to several ps, ending up in a thermal equilibrium of excited states independently from the initially excited state. However, global analysis of the 2DES data revealed that the pathways and dynamics of EET differ between plant LHCII and *B. corticulans*. An obvious change is that the longest resolved EET lifetime is around 5 ps in plant LHCII but 9.4 ps in *B. corticulans*. The EET process contributing mostly to the decay lifetime is from states around 669 nm – this spectral form is also resolved at 77 K and can be related to the ‘bottleneck’ long-lived Chls in plant LHCII. The 9.4 ps 2D DAS also revealed a fraction of long-lived Chl *b*, at 650–655 nm. Such long-lived Chl *b* states are not present in plant LHCII; therefore, the decay probably represents one of the extra Chl *b* molecules found in *B. corticulans*. It must be noted that the long-lived Chl *b* population has no significant impact on the overall rate of Chl *b* \rightarrow *a* EET at RT – the 2 ps average time for populating the lowest-energy Chl *a* is still very short, compared to the excitation lifetime of 4 ns. As discussed above, a second additional Chl *b* in *B. corticulans* LHCII absorbs at 658–659 nm. This spectral form rapidly relaxes by EET to Chl *a*, as revealed by the well resolved diagonal peak in the 260-fs 2D DAS (Fig. 8a).

As is the case with LHCII from higher plants [24], lowering the

Table 1

Decay lifetimes and relative amplitudes of the diagonal peaks in the 2D electronic spectra at 77 K.

Lifetime (ps)	650 nm	658 nm	669 nm	672 nm	674 nm
0.5	50%	51%	26%	8%	0%
2.7	22%	48%	50%	46%	40%
15.4	28%	1%	24%	46%	60%
Average lifetime (ps)	5.2	1.8	5.1	8.4	10.7
Average lifetime (<i>P. sativum</i>) ^a	2.5	4.2	3.5	4.5	5.7

^a from Akhtar et al. [24].

temperature to 77 K results in measurably slower EET dynamics in LHCI from *B. corticulans* as well. The relative contribution of decay lifetimes to the diagonal peaks in the 2D electronic spectra at 77 K is shown in Table 1. The average population lifetime of high-energy Chl *b* forms (650 nm) is about 5 ps (note that the final ns decay is not included in the calculation of the average lifetimes). EET from the 658-nm spectral form slows down as well – approximately equal amplitudes of the 0.5 ps and 2.7 ps lifetimes result in a 1.8 ps average lifetime. The slowest EET dynamics, however, is found in the Chl *a* region – with average lifetimes of 8.4 and 10.7 ps for the diagonal signals at 672 and 674 nm, respectively. Comparing these diagonal peak lifetimes with the values corresponding to LHCI from *P. sativum*, it is evident that EET can be up to two-fold slower in *B. corticulans*. An exception is the lifetime of the 658-nm peak, which is determined by relatively fast EET from the extra Chl *b*. The slower EET in the Chl *a* wavelength region may be intuitively understood in terms of comparatively lower Chl *a* concentration in the complex volume and lower density of excited states in energy domain. It can be said that adaptation of LHCI to shorter-wavelength light in the intertidal alga does come with a trade-off between the enhanced absorption cross-section and excitation migration time. Although exciton equilibration time is longer in *B. corticulans* – about 10 ps – it is still an order of magnitude shorter compared to the trapping time of PSII [50]. Therefore, the adaptive change should have negligible effect on the overall quantum efficiency.

5. Conclusions

The comprehensive spectroscopic characterization presented here reveals details on the adaptation of the siphonous alga *B. corticulans* to its intertidal habitat by spectrally tuning LHCI to shorter wavelengths. Compared to higher-plant LHCI, the complex contains two additional spectral forms of Chl *b* – absorbing at around 650 nm and 658 nm, at the expense of Chl *a* absorbing at around 674 nm and 679 nm – the lowest-energy Chl *a* form in LHCI. The specific Chl *a/b* exchange in *B. corticulans*, while retaining the general tertiary structure of the protein complex, presents a valuable opportunity to identify spectral forms and the associated Chl binding sites, which has been a highly challenging and contentious issue [15]. It would be highly informative to analyse the present spectroscopic results in terms of the complex structure, whenever it becomes determined, e.g. by X-ray diffraction or cryo-electron microscopy.

The adaptive change in Chl composition in *B. corticulans* LHCI alters the pathways and dynamics of EET. The Chl *b* form at 650 nm is relatively long-lived, slowing down EET to Chl *a*. The lower density of Chl *a* also results in a markedly slower EET to the lowest-energy state (677 nm), which occurs on a timescale of about 10 ps at 77 K. Thus, there is a trade-off between the increased absorption cross-section at shorter wavelengths and the excitation migration time. However, as the latter is much shorter than the overall excitation trapping time, the quantum efficiency of PSII should not be significantly affected. These results show that LHCI is a robust adaptable system whose spectral properties can be tuned to the environment while maintaining efficiency of EET.

Acknowledgements

The work is supported by grants from the Hungarian Ministry of Finance (GINOP-2.3.2-15-2016-00001), the National Research, Development and Innovation Fund (NKFI NN 124904; 2018-1.2.1-NKP-2018-00009), the Singapore Ministry of Education Academic Research Fund (MOE2015-T2-1-039), the National Key Research and Development Program of China (2017YFA0503700), a CAS Key Research Program for Frontier Science (QYZDY-SSW-SMC003), and the National Natural Science Foundation of China (31600191). CD measurements at the B23 beamline of the Diamond Light Source Ltd. were supported by the project CALIPSOplus under Grant Agreement 730872 from the EU Framework Programme for Research and Innovation HORIZON 2020.

Declaration of competing interest

The authors declare that they have no known competing financial interests or personal relationships that could have appeared to influence the work reported in this paper.

Appendix A. Supplementary data

Supplementary data to this article can be found online at <https://doi.org/10.1016/j.bbabi.2020.148191>.

References

- [1] J.T. Kirk, *Light and Photosynthesis in Aquatic Ecosystems*, 3rd edn., Cambridge University Press, Cambridge, 2011.
- [2] V. Giovagnetti, G. Han, M.A. Ware, P. Ungerer, X. Qin, W.-D. Wang, T. Kuang, J.-R. Shen, A.V. Ruban, A siphonous morphology affects light-harvesting modulation in the intertidal green macroalga *Bryopsis corticulans* (Ulvothales), *Planta* 247 (2018) 1293–1306.
- [3] G. Christa, S. Cruz, P. Jahns, J. de Vries, P. Cartaxana, A.C. Esteves, J. Seródio, S.B. Gould, Photoprotection in a monophyletic branch of chlorophyte algae is independent of energy-dependent quenching (qE), *New Phytol.* 214 (2017) 1132–1144.
- [4] H. Chen, S. Shen, Y. Liang, J. Leng, M. Tang, Y. Gong, Evidence for dissociation of chlorophyll *b* from the main light-harvesting complex in the oligomerization state isolated from marine alga, *Bryopsis corticulans*, *Biochim. Biophys. Acta* 1707 (2005) 170–178.
- [5] W. Wang, X. Qin, M. Sang, D. Chen, K. Wang, R. Lin, C. Lu, J.-R. Shen, T. Kuang, Spectral and functional studies on siphonaxanthin-type light-harvesting complex of photosystem II from *Bryopsis corticulans*, *Photosynth. Res.* 117 (2013) 267–279.
- [6] G. Chen, X. Niu, X. Chen, L. Li, T. Kuang, S. Li, Characterization of chlorophyll–protein complexes isolated from a Siphonous green alga, *Bryopsis corticulans*, *Photosynth. Res.* 96 (2008) 75–81.
- [7] K. Nakayama, M. Okada, Purification and characterization of light-harvesting chlorophyll *a/b*-protein complexes of photosystem II from the green alga, *Bryopsis maxima*, *Plant Cell Physiol.* 31 (1990) 253–260.
- [8] Z.F. Liu, H.C. Yan, K.B. Wang, T.Y. Kuang, J.P. Zhang, L.L. Gui, X.M. An, W.R. Chang, Crystal structure of spinach major light-harvesting complex at 2.72 Å resolution, *Nature* 428 (2004) 287–292.
- [9] A. Pagano, G. Cinque, R. Bassi, *In vitro* reconstitution of the recombinant photosystem II light-harvesting complex CP24 and its spectroscopic characterization, *J. Biol. Chem.* 273 (1998) 17154–17165.
- [10] R. Croce, T. Morosinotto, S. Castelletti, J. Breton, R. Bassi, The Lhca antenna complexes of higher plants photosystem I, *Biochim. Biophys. Acta* 1556 (2002) 29–40.
- [11] K. Nakayama, M. Mimuro, Chlorophyll forms and excitation energy transfer pathways in light-harvesting chlorophyll *a/b*-protein complexes isolated from the siphonous green alga, *Bryopsis maxima*, *Biochim. Biophys. Acta* 1184 (1994) 103–110.
- [12] K. Nakayama, M. Mimuro, Y. Nishimura, I. Yamazaki, M. Okada, Kinetic analysis of energy transfer processes in LHC II isolated from the siphonous green alga, *Bryopsis maxima* with use of picosecond fluorescence spectroscopy, *Biochim. Biophys. Acta* 1188 (1994) 117–124.
- [13] G.S. Schlau-Cohen, A. Ishizaki, G.R. Fleming, Two-dimensional electronic spectroscopy and photosynthesis: fundamentals and applications to photosynthetic light-harvesting, *Chem. Phys.* 386 (2011) 1–22.
- [14] F.D. Fuller, J.P. Ogilvie, Experimental implementations of two-dimensional Fourier transform electronic spectroscopy, *Annu. Rev. Phys. Chem.* 66 (2015) 667–690.
- [15] P.H. Lambrev, P. Akhtar, H.-S. Tan, Insights into the mechanisms and dynamics of energy transfer in plant light-harvesting complexes from two-dimensional electronic spectroscopy, *Biochim. Biophys. Acta* 2020 (1861) 148050.
- [16] P. Akhtar, D. Lindorfer, M. Lingvaj, K. Pawlak, O. Zsiros, G. Siligardi, T. Jávorki,

- M. Dorogi, B. Ughy, G. Garab, T. Renger, P.H. Lambrev, Anisotropic circular dichroism of light-harvesting complex II in oriented lipid bilayers: theory meets experiment, *J. Phys. Chem. B* 123 (2019) 1090–1098.
- [17] P. Akhtar, M. Lingvay, T. Kiss, R. Deák, A. Bóta, B. Ughy, G. Garab, P.H. Lambrev, Excitation energy transfer between light-harvesting complex II and photosystem I in reconstituted membranes, *Biochim. Biophys. Acta* 1857 (2016) 462–472.
- [18] P.J. Nowakowski, M.F. Khyasudeen, H.-S. Tan, The effect of laser pulse bandwidth on the measurement of the frequency fluctuation correlation functions in 2D electronic spectroscopy, *Chem. Phys.* 515 (2018) 214–220.
- [19] Z. Zhang, K.L. Wells, E.W.J. Hyland, H.-S. Tan, Phase-cycling schemes for pump–probe beam geometry two-dimensional electronic spectroscopy, *Chem. Phys. Lett.* 550 (2012) 156–161.
- [20] R. Bassi, M. Silvestri, P. Dainese, I. Moya, G.M. Giacometti, Effects of a non-ionic detergent on the spectral properties and aggregation state of the light-harvesting chlorophyll *a/b* protein complex (LHCII), *J. Photochem. Photobiol. B Biol.* 9 (1991) 335–353.
- [21] P. Lambrev, Z. Várkonyi, S. Krumova, L. Kovács, Y. Miloslavina, A.R. Holzwarth, G. Garab, Importance of trimer–trimer interactions for the native state of the plant light-harvesting complex II, *Biochim. Biophys. Acta* 1767 (2007) 847–853.
- [22] P. Akhtar, F. Göröf, G. Garab, P.H. Lambrev, Dependence of chlorophyll fluorescence quenching on the lipid-to-protein ratio in reconstituted light-harvesting complex II membranes containing lipid labels, *Chem. Phys.* 522 (2019) 242–248.
- [23] K.L. Wells, P.H. Lambrev, Z.Y. Zhang, G. Garab, H.-S. Tan, Pathways of energy transfer in LHCII revealed by room-temperature 2D electronic spectroscopy, *Phys. Chem. Chem. Phys.* 16 (2014) 11640–11646.
- [24] P. Akhtar, T.N. Do, P.J. Nowakowski, A. Huerta-Viga, M.F. Khyasudeen, P.H. Lambrev, H.-S. Tan, Temperature dependence of the energy transfer in LHCII revealed by two-dimensional electronic spectroscopy, *J. Phys. Chem. B* 123 (2019) 6765–6775.
- [25] T. Polívka, V. Sundström, Ultrafast dynamics of carotenoid excited states – from solution to natural and artificial systems, *Chem. Rev.* 104 (2004) 2021–2072.
- [26] R. Remelli, C. Varotto, D. Sandona, R. Croce, R. Bassi, Chlorophyll binding to monomeric light-harvesting complex - a mutation analysis of chromophore-binding residues, *J. Biol. Chem.* 274 (1999) 33510–33521.
- [27] T.N. Do, A. Huerta-Viga, P. Akhtar, H.L. Nguyen, P.J. Nowakowski, M.F. Khyasudeen, P.H. Lambrev, H.-S. Tan, Revealing the excitation energy transfer network of light-harvesting complex II by a phenomenological analysis of two-dimensional electronic spectra at 77 K, *J. Chem. Phys.* 151 (2019) 205101.
- [28] G. Zucchelli, P. Dainese, R.C. Jennings, J. Breton, F.M. Garlaschi, R. Bassi, Gaussian decomposition of absorption and linear dichroism spectra of outer antenna complexes of photosystem II, *Biochemistry* 33 (1994) 8982–8990.
- [29] G. Zucchelli, F.M. Garlaschi, R.C. Jennings, Thermal broadening analysis of the light harvesting complex II absorption spectrum, *Biochemistry* 35 (1996) 16247–16254.
- [30] G. Zucchelli, S. Santabarbara, R.C. Jennings, The Q_y absorption spectrum of the light-harvesting complex II as determined by structure-based analysis of chlorophyll macrocycle deformations, *Biochemistry* 51 (2012) 2717–2736.
- [31] V. Novoderezhkin, A. Marin, R. van Grondelle, Intra- and inter-monomeric transfers in the light harvesting LHCII complex: the Redfield–Förster picture, *Phys. Chem. Chem. Phys.* 13 (2011) 17093–17103.
- [32] F. Müh, M.E.-A. Madjet, T. Renger, Structure-based identification of energy sinks in plant light-harvesting complex II, *J. Phys. Chem. B* 114 (2010) 13517–13535.
- [33] H. Rogl, R. Schödel, H. Lokstein, W. Kühlbrandt, A. Schubert, Assignment of spectral substructures to pigment-binding sites in higher plant light-harvesting complex LHC-II, *Biochemistry* 41 (2002) 2281–2287.
- [34] K. Vrandečić, M. Rätsep, L. Wilk, L. Rusevich, M. Golub, M. Reppert, K.-D. Irrgang, W. Kühlbrandt, J.R. Pieper, Protein dynamics tunes excited state positions in light-harvesting complex II, *J. Phys. Chem. B* 119 (2015) 3920–3930.
- [35] Y. Miloslavina, P.H. Lambrev, T. Jávorf, Z. Várkonyi, V. Karlický, J.S. Wall, G. Hind, G. Garab, Anisotropic circular dichroism signatures of oriented thylakoid membranes and lamellar aggregates of LHCII, *Photosynth. Res.* 111 (2012) 29–39.
- [36] J.T. Nielsen, N.V. Kulminkaya, M. Bjerring, J.M. Linnanto, M. Rätsep, M.O. Pedersen, P.H. Lambrev, M. Dorogi, G. Garab, K. Thomsen, C. Jegerschöld, N.U. Frigaard, M. Lindahl, N.C. Nielsen, *In situ* high-resolution structure of the baseplate antenna complex in *Chlorobaculum tepidum*, *Nat. Commun.* 7 (2016) 12454.
- [37] H.-G. Kuball, E. Dorr, T. Höfer, O. Türk, Exciton chirality method. Oriented molecules – anisotropic phases, *Monatsh. Chem./Chem. Mon.*, 136 (2005) 289–324.
- [38] A. Natali, J.M. Gruber, L. Dietzel, M.C. Stuart, R. van Grondelle, R. Croce, Light-harvesting complexes (LHCs) cluster spontaneously in membrane environment leading to shortening of their excited state lifetimes, *J. Biol. Chem.* 291 (2016) 16730–16739.
- [39] L.O. Pålsson, M.D. Spangfort, V. Gulbinas, T. Gillbro, Ultrafast chlorophyll *b*-chlorophyll *a* excitation energy transfer in the isolated light harvesting complex, LHC II, of green plants. Implications for the organisation of chlorophylls, *FEBS Lett.* 339 (1994) 134–138.
- [40] T. Bittner, K.-D. Irrgang, G. Renger, M.R. Wasielewski, Ultrafast excitation energy transfer and exciton–exciton annihilation processes in isolated light-harvesting complexes of photosystem II (LHC II) from spinach, *J. Phys. Chem.* 98 (1994) 11821–11826.
- [41] J.P. Connelly, M.G. Müller, M. Hücke, G. Gatzert, C.W. Mullineaux, A.V. Ruban, P. Horton, A.R. Holzwarth, Ultrafast spectroscopy of trimeric light-harvesting complex II from higher plants, *J. Phys. Chem. B* 101 (1997) 1902–1909.
- [42] T. Bittner, G.P. Wiederrecht, K.-D. Irrgang, G. Renger, M.R. Wasielewski, Femtosecond transient absorption spectroscopy on the light-harvesting Chl *a/b* protein complex of photosystem II at room temperature and 12 K, *Chem. Phys.* 194 (1995) 311–322.
- [43] H.M. Visser, F.J. Kleima, I.H.M. van Stokkum, R. van Grondelle, H. van Amerongen, Probing the many energy-transfer processes in the photosynthetic light-harvesting complex II at 77 K using energy-selective sub-picosecond transient absorption spectroscopy, *Chem. Phys.* 210 (1996) 297–312.
- [44] F.J. Kleima, C.C. Gradinaru, F. Calkoen, I.H.M. van Stokkum, R. van Grondelle, H. van Amerongen, Energy transfer in LHCII monomers at 77 K studied by sub-picosecond transient absorption spectroscopy, *Biochemistry* 36 (1997) 15262–15268.
- [45] C.C. Gradinaru, S. Özdemir, D. Gülen, I.H.M. van Stokkum, R. van Grondelle, H. van Amerongen, The flow of excitation energy in LHCII monomers: implications for the structural model of the major plant antenna, *Biophys. J.* 75 (1998) 3064–3077.
- [46] M.A. Palacios, J. Standfuss, M. Vengris, B.F. van Oort, I.H.M. van Stokkum, W. Kühlbrandt, H. van Amerongen, R. van Grondelle, A comparison of the three isoforms of the light-harvesting complex II using transient absorption and time-resolved fluorescence measurements, *Photosynth. Res.* 88 (2006) 269–285.
- [47] A. Marin, I.N.M. van Stokkum, V.I. Novoderezhkin, R. van Grondelle, Excitation-induced polarization decay in the plant light-harvesting complex LHCII, *J. Photochem. Photobiol. A Chem.* 234 (2012) 91–99.
- [48] S.-J. Zhang, S.-C. Wang, J.-F. He, H. Chen, Energy transfer among chlorophylls in trimeric light-harvesting complex II of *Bryopsis corticulans*, *Acta Biochim. Biophys. Sin.* 38 (2006) 310–317.
- [49] P. Akhtar, C. Zhang, T.N. Do, G. Garab, P.H. Lambrev, H.-S. Tan, Two-dimensional spectroscopy of chlorophyll *a* excited-state equilibration in light-harvesting complex II, *J. Phys. Chem. Lett.* 8 (2017) 257–263.
- [50] S. Caffarri, K. Broess, R. Croce, H. van Amerongen, Excitation energy transfer and trapping in higher plant photosystem II complexes with different antenna sizes, *Biophys. J.* 100 (2011) 2094–2103.